Nanoscale

PAPER

View Article Online
View Journal | View Issue

Cite this: *Nanoscale*, 2015, **7**, 5665

Contact angle and adsorption energies of nanoparticles at the air–liquid interface determined by neutron reflectivity and molecular dynamics†

Javier Reguera,*[a,b,c] Evgeniy Ponomarev,[a] Thomas Geue,[d] Francesco Stellacci,[a] Fernando Bresme*[e] and Mauro Moglianetti*[f]

Received 27th January 2015,
Accepted 17th February 2015

DOI: 10.1039/c5nr00620a

www.rsc.org/nanoscale

Understanding how nanomaterials interact with interfaces is essential to control their self-assembly as well as their optical, electronic, and catalytic properties. We present here an experimental approach based on neutron reflectivity (NR) that allows the *in situ* measurement of the contact angles of nanoparticles adsorbed at fluid interfaces. Because our method provides a route to quantify the adsorption and interfacial energies of the nanoparticles *in situ*, it circumvents problems associated with existing indirect methods, which rely on the transport of the monolayers to substrates for further analysis. We illustrate the method by measuring the contact angle of hydrophilic and hydrophobic gold nanoparticles, coated with perdeuterated octanethiol (d-OT) and with a mixture of d-OT and mercaptohexanol (MHol), respectively. The contact angles were also calculated *via* atomistic molecular dynamics (MD) computations, showing excellent agreement with the experimental data. Our method opens the route to quantify the adsorption of complex nanoparticle structures adsorbed at fluid interfaces featuring different chemical compositions.

Introduction

The properties of nanoparticles (NPs) at the air–liquid, liquid–liquid and solid–liquid interfaces have attracted strong interest in the last few years for their scientific and technological importance.[1] A better understanding of these interfacial systems is crucial to shed light on complex physical processes like heterogeneous catalysis,[2] electron transfer,[3] biological surface activity,[4] biosensing[5] and self-assembly.[6] Understanding and controlling the adsorption of particles of dimensions below tens of nanometers at interfaces will help to design Pickering emulsions with longer stability,[6,7] to improve 2D supracrystals for catalytic applications with enhanced efficiency,[8,9] to stabilize self-assembled structures for surface-enhanced Raman spectroscopy detection of traces[10] and for nanoplasmonic applications.[11] Despite the great effort devoted to the investigation of the NP behavior at interfaces (adsorption, assembly and dynamics), a clear understanding of the rules governing nanoscale wetting phenomena is still an open challenge.[12]

Contact angle is a key parameter that defines the NPs affinity to adsorb at a fluid interface. It measures the relative height of the NP at the interface, which in turn determines the structure, dynamics and thermodynamic properties of NP monolayers. Contact angle (θ) is defined as the angle that the tangent to the NP surface makes with the interface measured through the liquid phase (Fig. 1b). Traditionally the contact angle has been measured using the sessile drop method.[13,14] Although it can be used to measure the contact angle of NPs deposited on substrates, it is not suitable for *in situ* measurements at fluid interfaces. The measurements performed on deposited NPs are influenced by the transfer process,[15,16] by the rearrangement of NPs and their shell on the substrate, by low coverage and roughness. Pinning and humidity are also major issues as they play a role in contact angle measurement.[17] More advanced techniques designed to overcome some of the problems associated with the sessile drop method, have been used recently to measure contact angles and interfacial ener-

[a]*Institute of Materials, École Polytechnique Fédérale de Lausanne, 1015 Lausanne, Switzerland. E-mail: jreguera@cicbiomagune.es*
[b]*CIC BiomaGUNE, Paseo de Miramón 182C, 20009 Donostia-San Sebastian, Spain*
[c]*Ikerbasque, Basque Foundation for Science, 48011 Bilbao, Spain*
[d]*Laboratory for Neutron Scattering and Imaging, Paul Scherrer Institut, 5232 Villigen, Switzerland*
[e]*Department of Chemistry, Imperial College, SW7 2AZ London, United Kingdom. E-mail: f.bresme@imperial.ac.uk*
[f]*Center for Biomolecular Nanotechnologies (CBN), Istituto Italiano di Tecnologia, 73010 Arnesano, Italy. E-mail: mauro.moglianetti@iit.it*

†Electronic supplementary information (ESI) available: TEM images, NR geometrical model, Simulation procedure. χ^2 graph and table of Janus model in NRW and CMAu. See DOI: 10.1039/c5nr00620a

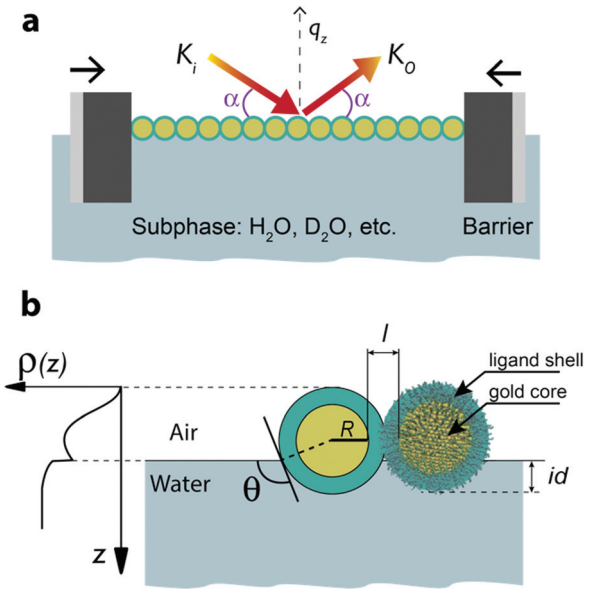

Fig. 1 Scheme of the experimental setup showing the NR on a NP monolayer. (a) NPs forming a monolayer at the air–water interface in a Langmuir–Blodgett trough. NR is measured *in situ* on this monolayer using contrast variation of the aqueous subphase. (b) Model of the core–shell NPs at the interface where θ is the contact angle, R and l are the NP core radius and the interparticle distance (measured by TEM), *id* the immersion depth, and $\rho(z)$ is the calculated scattering length density profile.

gies. Gel Trapping Technique (GTT) has been used to investigate the interfacial properties of NPs trapped on PDMS using Atomic Force Microscope (AFM) and Scanning Electron Microscopy (SEM).[18,19] AFM, operating in the small amplitude mode, has been used to map the solid–liquid adhesion energies of the deposited gold NPs.[20,21] A method based on freeze-fracture shadow-casting cryo-scanning electron microscopy has also been recently proposed, which allows measurements of contact angles of large NPs, with diameters higher than ten nanometers.[22] Ellipsometric measurements have been performed to obtain the contact angle of metallic NPs covered by a polymeric shell.[23] Despite the development of these new techniques, it still remains extremely challenging to measure the contact angle of core–shell NPs of few nanometers directly at air–water interfaces.

X-ray and neutron scattering techniques have shown a great potential in providing detailed picture of complex materials at interfaces.[24–26] Mohwald *et al.*[27] used X-ray reflectivity to characterize the adsorption layer of NPs at the air/water interface and to quantify the layer thickness on a Langmuir trough. Calzolari *et al.*[28] used X-ray reflectivity to investigate the structure of NP monolayers *in situ* at water–hexane interface. In this work they had determined the immersion depth and contact angles of the NP (silica) core. Isa *et al.* expanded this work to address the influence of the NPs shell architecture in determining the monolayer interfacial microstructure.[29] *In situ* high-energy X-ray reflectivity was used to quantify the vertical position and inter-particle spacing of core–shell iron oxide poly(ethylene glycol) (PEG) NPs adsorbed at water–*n*-decane interfaces. These studies, however, could not be used to directly extract information of the ligand shell covering metallic NPs, as the contribution of the metallic core to the X-ray scattering is overwhelming making impossible to detect the weak scattering of the shell.

Molecular Dynamics (MD) simulations have been used to determine the contact angle of gold nanoclusters covered by an alkylthiol self-assembled monolayer (SAM) at the air–water interface. Simulations showed that the length of the alkylthiol profoundly influences their wetting behavior.[30] Particles covered by butanethiol, dodecanethiol and octadecanethiol were found to be stable at the air–water interface, possessing large, well-defined contact angles. Simulation studies also demonstrated how the length of the surfactant chain deeply influences the wetting behavior of the NPs as the configuration of the shell composed of ligands with a length that is relatively higher than the dimension of the core was strongly perturbed by the interface. MD simulations have also been employed to quantify the impact of the line tension on the contact angle of model NPs at liquid–vapor interfaces. It was found that generally the line tension has a minor impact on the contact angles of particles with radius larger than ~1 nm.[31]

In this report we present NR experiments combined with the contrast variation method to *in situ* measure the contact angle of NPs deposited on a Langmuir–Blodgett trough at close-packed configuration and at the air–water interface. We present a new approach that enables the determination of contact angles, adsorption energies and interfacial energy differences of core–shell NPs. NR offers several advantages compared to X-rays,[32,33] particularly for core–shell metallic NPs. The contrast variation method offers the possibility to perdeuterate the ligands on the shell. In this way the neutron scattering length density of the perdeuterated organic shell is higher than that of the metallic core and this makes it possible to precisely define the shell/media interface. NR has also the advantage that the neutron "contrast variation" method can be applied to the liquid subphase in order to obtain different reflectivity profiles of the same system. This guarantees the uniqueness of the solution in the numerical modeling of the NR data. The contrast variation method offers also the possibility to selectively perdeuterate one of the ligands on binary-ligand shells allowing the determination of ligands phase separation (*i.e.* Janus) eventually present at the surface of the NPs. All this makes NR the technique of choice to obtain a precise and detailed picture of the metallic NPs shell structure at the water–air interface.

Until now there have been only a few studies on the investigation of NPs using NR and Langmuir troughs. These studies have focused mainly on multicomponent polymer–NP systems.[34,35] Rezende *et al.* studied the structural evolution of a Langmuir layer consisting of gold NPs grafted with thermo sensitive poly(*N*-isopropyl acrylamide). The structural changes induced by polymer temperature coil–globule transition were investigated. Ujihara *et al.* used NR on a Langmuir trough to analyze the relative composition and disposition of a compo-

site Langmuir film consisting of gold NPs and amphiphilic dendrimer molecules at the air–water interface.[35] These studies did not attempt to estimate contact angles and the interfacial properties of the hybrid material, but rather focused on the structure of the hybrid material at the interface.

In this work we focus on gold NPs covered by a SAM of thiolated molecules. The SAM, or ligand shell, imparts specific functionality to the NP, such as solubility, and modulation of its interactions with other particles, which influence their self-assembly into complex structures. In addition, the NP can be coated with mixtures of ligands which bring in different functionalities allowing for example a fine control of the NP solubility providing at the same time labeling, catalytic or bioactive properties. It has been pointed out in different papers that these ligands can arrange themselves into surface domains (patches), hence providing new interfacial properties to the NPs.[36–38] Among these arrangements, Janus (two different sides), narrow nanodomains (stripes) and uniformly mixed morphologies have been reported in experimental and theoretical papers.[39–41] The size of NPs, chemical nature of the ligands and their arrangement at the surface affect their interaction with interfaces and therefore their use in different applications.

Here, we present a report on a new approach to measure *in situ* the contact angle, interfacial, and adsorption energies of NPs coated either by one hydrophobic ligand or by a mixture of two different ligands hydrophobic–hydrophilic on a Langmuir–Blodgett trough. Molecular dynamics simulations are employed simultaneously to compute the contact angle, hence providing a direct comparison with the NPs atomistic structure at the water surface. We demonstrate that our approach can be used to differentiate between NPs in which the ligands are segregated forming a Janus configuration from NPs where the ligands are uniformly mixed or form small sub-nanometer domains. Our approach can in principle be applied to other kinds of complex NPs or NPs that are adsorbed from one of the phases to the liquid/liquid or liquid/vapor interface.

Results and discussion

Two sets of NPs have been used, one coated by a single ligand, perdeuterated 1-octanethiol (d-OT) and the other one coated by two ligands, perdeuterated 1-octanethiol and 6-mercapto-1-hexanol (d-OT : MHol 1 : 1). In the latter case the two different ligands self-assemble to form narrow stripe-like nanodomains on the surface and confer to the NPs different interfacial properties.[20] The perdeuterated ligand was used to highlight the shell of the NP with respect to the gold core as the perdeuterated ligand has higher scattering length density, hence allowing a clear definition of the NP–solvent interface. In the case of two ligands the selective deuteration of one of the ligands is used to increase the contrast between them and is not expected to produce a significant difference on the contact angle of the NP.

The NPs were dissolved in chloroform and deposited on top of a water phase on a Langmuir trough. The solvent was left to evaporate and the compression was performed up to the beginning of the solid phase before NR measurements were performed (Fig. 1a and Experimental section). We ensure by visual inspection the absence of buckling or monolayer collapse, and Transmission Electron Microscopy (TEM) grids were taken through Langmuir–Schaefer deposition to establish the good quality of the film. Several liquid subphases with different contrast (a mixture of D_2O and H_2O with different scattering length density depending on the ratio) were employed to highlight the different characteristics of the monolayer, hence providing several independent measurements of the same system. This approach allows the validation of the method as different contrasts give different information on the system and is able to produce higher precision in the contact angles due to acquisition of reflectivity profiles on different subphase.

Once the NR experiment was performed the reflectivity profiles were modeled using the following construction: NPs were represented as core–shell structures with spherical gold cores arranged in a 2D hexagonal lattice (Fig. 1b). The core diameter and interparticle distance were obtained from the TEM images of the 2D supracrystal. The scattering length density profile was obtained dividing the sample into several thin slabs of 1 Å parallel to the interface. For each slab the scattering length density (SLD) is calculated as a weighted average SLD of the different materials and their relative contribution. The stratified matrix was input in the Motofit software[42] and compared with the experimental results. The χ^2 obtained in Motofit was used to evaluate the best model and best fit to the experimental data. The contact angle θ of the NPs at the air–liquid interface was obtained from the immersion depth *id*. More details about the model (including some refinements to treat the NP polydispersity and the effects of polydispersity of interparticle distance) are reported in the ESI.†

Homoligand NPs (d-OT)

For homoligand NPs coated with d-OT, reflectivity data were collected with 3 different subphase contrasts (Fig. 2a). In order to obtain structural and geometrical information about the NP monolayer at the air–liquid interface, we developed a model to obtain the best fit to the experimental data. Modeling started from null-reflecting water contrast (NRW), that is, the contrast at which scattering length densities of water and air are matched. This contrast contains information of the NP monolayer only, as the two media do not contribute to the scattering. This contrast was used to validate the agreement between the experimental results and the analytical model based on the geometric information obtained from TEM image analysis. The other two contrasts (D_2O and "contrast match gold" (CMAu) *i.e.* water with the same SLD as gold) give information on the immersion depth of the NPs and therefore the contact angle. The fitting was performed by considering different contact angles in order to minimize χ^2 (goodness of fit or weighed sum of square of residuals)[42] for the two contrasts. The resulting reflectivity curves for the D_2O and CMAu contrasts corresponding to the lowest value of χ^2 are shown in Fig. 2a. The value of the contact angle for CMAu varies from

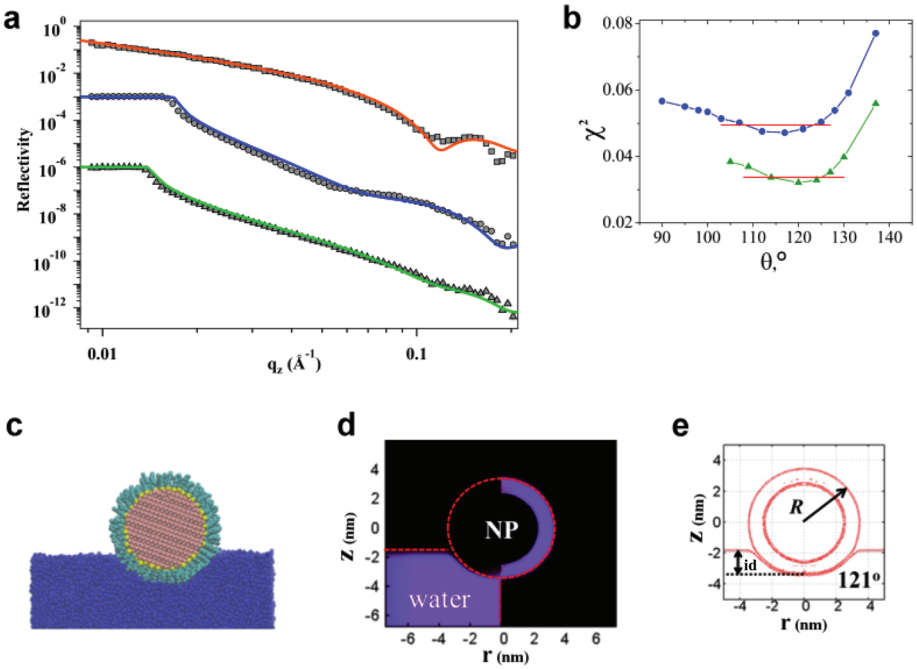

Fig. 2 (a) Reflectivity curves for d-OT-coated NP monolayer. Experimental results are shown with symbols and the model (best fit) with solid lines for three different contrasts: NRW in red, D_2O in blue and CMAu in green. (b) Fitting parameter χ^2 as a function of contact angle for d-OT-coated NPs for D_2O in blue and CMAu in red. The error of the angle indicated with the red line was chosen with $\chi^2 = 1.05\ \chi_{min}{}^2$. (c) Snapshots of equilibrated configurations of Au_{3832}–d-OT_{476} (only atoms with $y < 0$ (y axis is normal to the plane) are represented). (d) Density profile indicating the water level on the left and the ligands on the right. (e) Contour line and contact angle measured from the immersion depth.

114° to 125° for an error interval of $\chi^2 \leq 1.05\ \chi_{min}{}^2$. In the same way, for D_2O contrast, the contact angle varied from 108° to 125°. The dependence of χ^2 with the contact angle employed in the fit is shown in Fig. 2b. The overlap between the two error intervals can be used to further refine the measurement to an interval of 119.5 ± 5.5°.

Molecular dynamics simulations were employed to determine the contact angles of 4.8 nm d-OT covered NPs (Au_{3832}–dOT_{476}). Fig. 2c shows a snapshot of an equilibrated configuration while Fig. 2d shows the corresponding density profile (water in the left part and ligands on the right part). From this snapshot it is clearly visible that the NP prefers the air phase due to its hydrophobic nature and that there is no noticeable deformation of the ligand shell. This result validates the assumptions taken in the geometric model that models NPs as spheres (with only lateral deformation due to neighboring NPs). Fig. 2e shows the contour lines of the NP and the interface where *id* and *R* stand for the immersion depth and the NP radius (including the organic layer) respectively. We have used this density profile contours to estimate the NP contact angles by using a geometrical construction[30] which requires both the NP radius and the depth of immersion in the water phase, $\cos\theta = id/R - 1$. The results obtained by simulation are shown in Table 1. Good agreement is found between the experimental and the simulation contact angles (119.5° determined experimentally and 121° determined from the simulations). To make our simulation more comparable to the experimental NP monolayer we simulated a cluster consisting of 7 NPs and compared the contact angles of the NP in the center of the cluster with the ones on the sides (see ESI†). The results showed a contact angle of 125 and 121° respectively, similar to the contact angle obtained from the simulation of a single NP, and in good agreement with the NR experimental results.

Table 1 Physical model parameters for NR and MD

	d-OT		d-OT–MHol 1 : 1	
	NR	MD	NR	MD
$d_c{}^a$ (nm)	4.8 ± 0.4	4.85	4.7 ± 1.0	4.85
$d_{NP}{}^b$ (nm)	7.0 ± 0.4	7.01	6.9 ± 1.0	7.01
$l_{NP-NP}{}^c$ (nm)	1.5 ± 0.4	1.31	1.4 ± 0.6	1.35
C. ang.^{d} (θ)	119.5 ± 5.5	121 ± 2	85 ± 10	77 ± 2
$-\Delta E_{water}{}^e$ (kT)	1500 ± 240	1549 ± 61	545 ± 260	406 ± 36
$-\Delta E_{air}{}^f$ (kT)	173 ± 60	158 ± 20	773 ± 334	1013 ± 56
$\gamma_2 - \gamma_1{}^g$ (mN m^{-1})	−35.5 ± 6.0	−37.1 ± 2.2	6.3 ± 12.5	16.2 ± 2.4

[a] Average core diameter (±standard deviation, s.d.). [b] Average NP diameter ± s.d. [c] Average edge-to-edge distance ± s.d. [d] Contact angle (±error interval taken as 1.05 $\chi_{min}{}^2$ for NR, and ± standard error for MD). [e] Adsorption energy from water, energy necessary to move a NP from the interface to the water phase (kT has been taken as 4.11×10^{-21} J). [f] Adsorption energy from air, energy necessary to move a NP from the interface to the air phase (kT has been taken as 4.11×10^{-21} J). [g] Difference between interfacial energies of NP/water and NP/air.

Interfacial energies were calculated from the contact angle of d-OT NPs according to Young's equation: $\cos\theta = (\gamma_2 - \gamma_1)/\gamma_0$ where γ_0 is the air/liquid interfacial free energy (also called surface tension) and $\gamma_2 - \gamma_1$ is the difference in interfacial free energies (energy to create an interface per unit area) between

NP/liquid and NP/vapor. Hence, this free energy quantifies the preference of the NPs for one phase *versus* the other one. The adsorption energy ΔE of a NP at the interface has been quantified from the NP's contact angle. For spherical particles of radius r adsorbed at an interface with interfacial tension γ_0 the adsorption energy is $\Delta E = -\pi r^2 \gamma_0 (1 \pm \cos\theta)^2$ with the sign inside the bracket negative for removal into the water phase, and positive for removal into the air (or oil phase).[43,44] Numerical data for the contact angles and adsorption and interfacial energies for NR measurements and simulations are summarized in Table 1.

Mixed ligand NPs (d-OT : MHol 1 : 1)

Reflectivity data obtained for mixed-ligand coated NPs were also analyzed. The shell of the NPs consists of two different ligands, d-OT with hydrophobic properties and MHol with hydrophilic properties. In our model we assume that ligands are uniformly distributed on the NP surface although stripes-like domains have been previously observed.[20] A uniform composition is a valid assumption because NR has a sub-nanometer resolution in the z-axis but not on the horizontal plane. The experimental system is also made by a large number of NPs with different orientations and with irregularities in the nanodomain formation,[41] as a consequence the difference between uniformly mixed and small nanodomain or stripe structure is not detectable.

Results of experiment and modeling are shown in Fig. 3a for two contrasts, NRW that is used to validate the model, and CMAu contrast that is used for the calculation of the contact angle. In a similar way as for d-OT NPs we have calculated the χ^2 for different contact angles (Fig. 3b) and a confidence interval is taken to obtain the experimental contact angle. This contact angle is 85 ± 10° that is much lower than that of d-OT NPs as expected due to the presence of hydrophilic ligands.

This result is in good agreement with the value obtained from our molecular dynamic simulation of NPs coated with an organic layer of uniformly distributed ligands (Au_{3832}–d-OT_{218}–$MHol_{218}$). Fig. 3c shows a snapshot of an equilibrated NP immersed mainly in the water phase due to the hydrophilic character of the NP. The analysis of the contour density shows a value of 77° that is within the error range of the experimental value (Fig. 3e). Furthermore, for the case of a cluster of 7 NPs (see ESI†) the simulation shows an increase in the angle of 85 and 81° for the NP in the center of the cluster and in the periphery respectively, which brings the simulation values closer to the experimental measurements of the monolayers.

Adsorption and interfacial energies have been calculated from the contact angle of d-OT : MHol 1 : 1. The results of these energies together with the ones obtained from simulations are summarized in Table 1.

As discussed above NR cannot detect the presence of ligand nanodomains not large enough to orient the NPs. However, the NR profile can detect the presence of domains like those formed in amphiphilic Janus NPs, where each domain is preferentially immersed in one of the two media and the domain boundary is parallel to the interface. This Janus morphology can be obtained during the synthesis and it is driven by the interplay of enthalpic and entropic effects[39] as well as kinetic

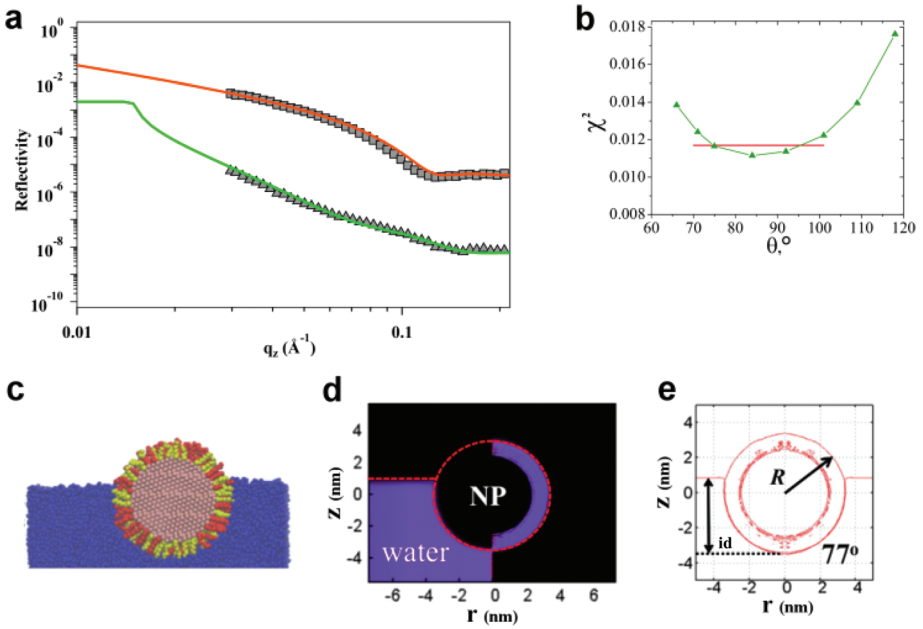

Fig. 3 (a) Reflectivity curves for d-OT–MHol 1 : 1 coated NP monolayer. Experimental results are shown with symbols and the model (best fit) with solid lines for two different contrasts, NRW in red and CMAu in green. (b) Fitting parameter χ^2 as a function of contact angle for the contrast CMAu. The error of the angle indicated with the red line was chosen with $\chi^2 = 1.05\ \chi_{min}^2$. (c) Snapshots of equilibrated configurations of Au_{3832}–d-OT_{218}–$MHol_{218}$ (red-d-OT; yellow-MHol) (only atoms with $y < 0$ (y axis is normal to the plane) are represented). (d) Density profile indicating the water level on the left and the ligands on the right. (e) Contour line and contact angle measured from the immersion depth.

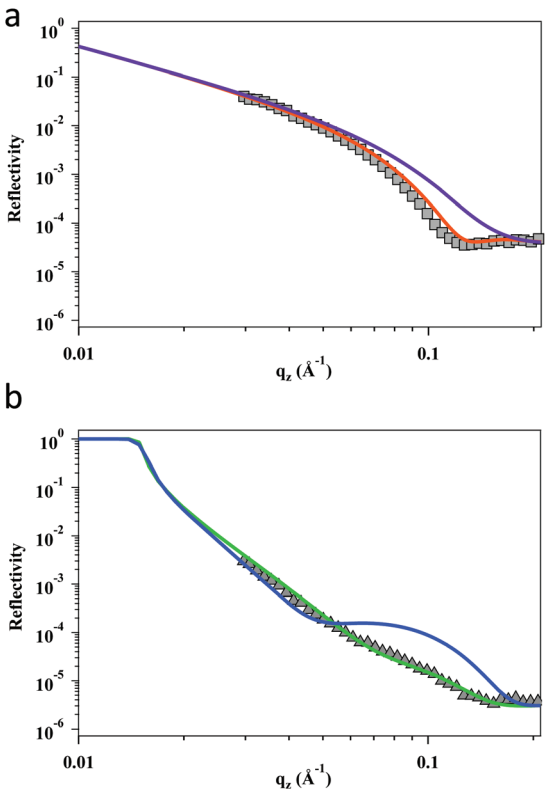

Fig. 4 Comparison of two models of SAMs with Janus structure and uniform distribution of ligands for d-OT–MHol 1 : 1 coated NPs in two different subphases. (a) NR profile (squares) in NRW subphase with two different models (solid lines): uniformly mixed in red and Janus in violet. (b) NR profile (triangles) in CMAu subphase, showing the best two fits (solid lines) for uniformly mixed in green (θ = 84°) and Janus in blue (θ = 97°).

effects.[45,46] To test the possible existence of Janus NPs in our monolayers, we modeled the NPs with Janus nanodomain structure (see ESI†) and fitted the experimental data to this model. The results are shown in Fig. 4. A considerable mismatch between the modeled curve for the Janus structure and the experimental points is observed for NRW where the model is independent of the contact angle. Also the best fit for CMAu shows a considerable mismatch (Fig. 4b). Furthermore, the calculated values of the fitting parameter χ^2 for the Janus case are one order of magnitude higher than those for the uniformly mixed case (see ESI, Table S1†). This mismatch strongly suggests that the Janus shell configuration is not present in our NPs.

Discussion

The key result of our work is the *in situ* determination of the three-phase contact angle of passivated metallic NPs at the air–water interface. The contact angle for d-OT-coated NPs is in line with the values obtained in previous theoretical reports of alkanethiol NPs. Tay and Bresme[30] reported using molecular dynamics simulations a contact angle of 115° for butanethiol and 140° for dodecanethiol coated gold clusters Au_{140}. Our result for NPs covered by an alkanethiol with an intermediate length between those two ligands shows a contact angle value (~120°) that lies in that range despite the difference in the NP core size. One important consideration of Tay and Bresme's work is that they observed a deformation of the shell, that changed from a purely spherical into a lens-like shape for long ligands, giving rise to two contact angles.[30] This effect arises probably from the large thiol length/core radius ratio that increases the space between ligands on the parts separated from the core allowing a bigger deformation. In the NPs investigated in this work (Au_{3832}–d-OT_{476}), that involves a smaller length/core radius ratio, we do not observe significant deformations. Even in the case of smaller NP sizes like Au_{1289}–OT_{251} (core diameter ~3.5 nm) this deformation is still small (see ESI†). This result validates the geometrical model we have developed to analyze the NR data. The NP deformation could be an important factor that will need to be taken into consideration to model the NR data of NPs involving large ligand length/core radius ratio.

The contact angle obtained for d-OT : MHol NPs is lower than the one of d-OT NPs as the presence of hydrophilic groups at the surface of the NPs lowers the hydrophobicity of the NPs. In this case the simulations show slightly smaller values than the experiment, which still lies within the experimental error of our NR data (Table 1). Also, the MD simulation shows that the Au_{3832}–d-OT_{218}–$MHol_{218}$ does not feature shell deformation validating the geometrical model applied to the NR experiment.

Comparison of our results with other experimental reports based on the traditional sessile drop method poses some issues as discussed in the Introduction. We believe that the comparison between the values obtained using our method and the traditional sessile drop ones present in the literature have only limited validity as the latter does not measure the NPs in the same state. NR measures directly at the air–water interface while in other methods the NPs are deposited and dried on a solid substrate with all the consequent problems. On the other hand, sessile drop measurements performed on similar NPs have shown different results than ours, ~84° for a substrate covered by 1-octanethiol (OT) NPs and ~68° for a substrate covered by OT : MHol 1 : 1 NPs.[20] In a sessile drop experiment performed with our NPs deposited with Langmuir–Schaefer on a glass slide, we obtained a contact angle of 104 ± 3° for d-OT and 86 ± 3° for d-OT : MHol (see ESI†). The discrepancy with these results and the ones present in the literature, both transferred to a dry substrate, can be attributed to the different sample preparation. The contact angle on SAMs present on flat surfaces has a value of 107° for OT.[47] This value can be considered in line with our results. For the case of d-OT : MHol 1 : 1 using values present in the literature for homoligand SAMs on flat surfaces, a value of ~70° can be inferred.[47] Again, great care has to be taken in performing a comparison between these results, given that the two systems are highly different for the presence of NPs curvature and NPs higher density of ligands.[48,49]

Regarding adsorption energies, all the NPs show values between two and three orders of magnitude higher than kT. This indicates a strong adsorption of the NPs to the interface and very low probability of the NPs to abandon it. The energies of adsorption from water (ΔE_{water}), *i.e.*, the energy necessary to move the NP from the interface to the water phase, decreases around three times with the substitution of half of the hydrophobic ligands by the hydrophilic ones even though NPs have sufficient energy values to strongly adsorb at the interface (~550 kT). We have also included the values of ΔE_{air}, which can be of interest for experiments where a different phase is used. Unlike in ΔE_{water}, which is a property of the NP, $\gamma_2 - \gamma_1$ is an intrinsic property of the surface of the NP and reflects the difference in interfacial free energy of the NP/water and NP/air interfaces. d-OT NPs feature a negative and relatively high value of $\gamma_2 - \gamma_1$ indicating a tendency of the surface to be surrounded by air. On the other hand d-OT : MHol 1 : 1 NPs have a slightly positive value of $\gamma_2 - \gamma_1$ showing a similar tendency of the surface of the NP to be covered by water or air (this value can be also negative within the error range).

Experimental section

Nanoparticle synthesis

d-OT coated gold NPs. Gold NPs covered with different alkane thiols were synthesized using a modification of the method described by Zheng *et al.*[26,50] 0.25 mmol chloro(triphenylphosphine) gold was dissolved in 20 mL of benzene and 0.5 mmol of ligands (perdeuterated 1-octanethiol (d-OT)) was added and mixed for 10 min. After that, 2.5 mmol of a borane *tert*-butylamine complex dissolved in 20 mL of benzene was added to reduce the sample. Once added, the solution was put immediately to reflux at 150 °C and left to react for one hour under strong stirring. The sample was precipitated with methanol and the purification was made in at least five cycles of centrifugation with acetone.

d-OT–MHol 1 : 1 coated gold NPs. A Procedure similar to the d-OT NPs was used. 0.25 mmol chloro(triphenylphosphine) gold was dissolved in 20 mL of toluene–methanol 1 : 1 (v/v) and 0.25 mmol of ligands (0.125 mmol of perdeuterated 1-octanethiol (d-OT) and 0.125 mmol of 6-mercapto-1-hexanol (MHol)) was added and mixed for 10 min. After that 2.5 mmol of a morpholine borane complex dissolved in 20 mL of toluene–methanol 1 : 1 (v/v) was added to reduce the sample. Once added, the solution was put immediately to reflux at 95 °C and left to react for one hour under strong stirring. The sample was precipitated with toluene and the purification was made in at least five cycles of centrifugation with acetone. The final ratio of the two ligands is expected to correspond with the one used during the synthesis based on NMR characterization of the hydrogenous equivalent NPs.

Transmission electron microscopy

TEM images were taken in a Philips/FEI CM12 operating at 120 kV or a FEI Tecnai Spirit at 100 kV. The images were analyzed using the Image-J software package [http://rsbweb.nih.gov/ij/].

To measure the diameter and interparticle distance, the images were transformed to binary using the default threshold. The module of particle analysis was used to produce the area and the center of mass of every particle. The diameter and the diameter distribution were obtained from the areas assuming that the particles were spherical and averaging to all the diameters. To measure the interparticle distance the center-to-center distances between all the centers of mass on the TEM images were calculated and represented in a histogram. The interparticle distance was calculated averaging the distances of the first peak of the histogram. The edge-to-edge distance was equally calculated as the average of the edge-to-edge distances obtained as the center-to-center distance minus the sum of the two NPs radii.

Neutron reflectivity (NR)

NP solution was prepared by dissolving the NPs in chloroform (at a concentration of 1 mg mL^{-1}). Great care was also taken to use completely dissolved NPs and to avoid the formation of a collapsed phase in the Langmuir isotherm avoiding in this way the presence of aggregates or double and triple layers. The NR measurements were conducted on AMOR beam line at Paul Scherrer Institute (PSI) in Villigen (CH) and on INTER beam line at ISIS (UK). The experiment was carried out on a Langmuir–Blodgett trough equipped with a moving barrier. The NP solution was spread on the water interface. After deposition, the solvent was allowed to evaporate for 10 minutes before starting the compression. The NP monolayer area was decreased up to a surface pressure of 12 mN m^{-1}. After reaching this value the barrier compression was stopped (constant area) and NR data were collected. Three subphases with different scattering length density were used: deuterated water (D_2O) with SLD = 6.33×10^{-6} $Å^{-2}$; mixtures of deuterated and hydrogenous water with SLD = 0 defined as null-reflecting water (NRW) and mixtures of deuterated and hydrogenous water with SLD = 4.5×10^{-6} $Å^{-2}$ that matches the gold core of a NP, defined as CMAu contrast. Surface pressure was controlled by a Wilhelmy plate. Samples for TEM were taken using the Langmuir–Schaefer method on carbon-coated grids immediately after the compression, and after the NR was finished. No significant difference was observed in the diameter or the interparticle distance before and after the NR experiment.

The NR profiles were fitted to a geometrical model (more details in ESI†). The fit was performed using the software package Motofit.[42]

Conclusions

We have presented a new experimental approach to determine interfacial properties of NPs coated with an organic shell at the air–liquid interface. Our method is based on the NR technique, which has enabled us to directly measure for the first time the three-phase contact angle directly *in situ* in a NP

monolayer supported on a Langmuir trough. We have further used atomistic computer simulations to validate the model used to analyze the NR data, and to visualize the structure of the NP shell in contact with the water surface. The experimental results are comparable to the ones obtained with molecular dynamics simulation.

The methodology described in this paper should have a significant impact on nanoscale interfacial science, given the increasing importance of NP adsorption at fluid interfaces in the manufacture of self-assembled monolayers for uses in plasmonics, sensors or catalysis. Our work provides to the scientific community a tool to *in situ* measure the interfacial properties of NPs. We envision that our method can be extended to investigate NPs of complex shapes, and different core–shell chemistries, which feature a more complex wetting behavior than spherical homogeneous NPs. With a modification of the experimental setup, it should also be possible to quantify the contact angle of NPs adsorbed at liquid–liquid interfaces. Overall our method opens the route to address the high demand for a better understanding of the interfacial phenomena of the nanoscale complex systems.

Acknowledgements

We thank the Swiss National Science Foundation for financial support. We thank John Webster for the fruitful help and discussions. We thank Paul Scherrer Institute (CH) and ISIS-Rutherford Appleton Laboratory (UK) for providing beamtime at AMOR and Inter. FB would like to thank the EPSRC (EP/J003859/1) for the award of a Leadership Fellowship.

Notes and references

1 A. Maestro, E. Guzmán, F. Ortega and R. G. Rubio, *Curr. Opin. Colloid Interface Sci.*, 2014, **19**, 355–367.
2 S. Crossley, J. Faria, M. Shen and D. E. Resasco, *Science*, 2010, **327**, 68–72.
3 B. Oregan and M. Gratzel, *Nature*, 1991, **353**, 737–740.
4 A. Verma and F. Stellacci, *Small*, 2010, **6**, 12–21.
5 J. N. Anker, W. P. Hall, O. Lyandres, N. C. Shah, J. Zhao and R. P. Van Duyne, *Nat. Mater.*, 2008, **7**, 442–453.
6 A. Boker, J. He, T. Emrick and T. P. Russell, *Soft Matter*, 2007, **3**, 1231–1248.
7 S. Sacanna, W. K. Kegel and A. P. Philipse, *Phys. Rev. Lett.*, 2007, **98**, 158301.
8 J. S. Mu, L. Zhang, M. Zhao and Y. Wang, *ACS Appl. Mater. Interfaces*, 2014, **6**, 7090–7098.
9 A. Ghosh, F. Stellacci and R. Kumar, *Catal. Today*, 2012, **198**, 77–84.
10 M. P. Cecchini, V. A. Turek, J. Paget, A. A. Kornyshev and J. B. Edel, *Nat. Mater.*, 2013, **12**, 165–171.
11 P. P. Fang, S. Chen, H. Q. Deng, M. D. Scanlon, F. Gumy, H. J. Lee, D. Momotenko, V. Amstutz, F. Cortes-Salazar, C. M. Pereira, Z. L. Yang and H. H. Girault, *ACS Nano*, 2013, **7**, 9241–9248.
12 D. Chandler, *Nature*, 2005, **437**, 640–647.
13 Y. D. Guo, D. Y. Tang, Y. C. Du and B. B. Liu, *Langmuir*, 2013, **29**, 2849–2858.
14 P. M. Hansson, L. Skedung, P. M. Claesson, A. Swerin, J. Schoelkopf, P. A. C. Gane, M. W. Rutland and E. Thormann, *Langmuir*, 2011, **27**, 8153–8159.
15 R. Banerjee, M. K. Sanyal, M. K. Bera, A. Singh, J. Novak and O. Konovalov, *Phys. Rev. E: Stat. Phys., Plasmas, Fluids, Relat. Interdiscip. Top.*, 2011, **83**, 051605.
16 S. Kundu, K. Das and O. Konovalov, *AIP Adv.*, 2013, **3**, 092130.
17 J. N. Israelachvili, *Intermolecular and surface forces*, Academic Press, Burlington, Mass, 3rd edn, 2011.
18 V. N. Paunov, *Langmuir*, 2003, **19**, 7970–7976.
19 L. N. Arnaudov, O. J. Cayre, M. A. C. Stuart, S. D. Stoyanov and V. N. Paunov, *Phys. Chem. Chem. Phys.*, 2010, **12**, 328–331.
20 J. J. Kuna, K. Voitchovsky, C. Singh, H. Jiang, S. Mwenifumbo, P. K. Ghorai, M. M. Stevens, S. C. Glotzer and F. Stellacci, *Nat. Mater.*, 2009, **8**, 837–842.
21 K. Voitchovsky, J. J. Kuna, S. A. Contera, E. Tosatti and F. Stellacci, *Nat. Nanotechnol.*, 2010, **5**, 401–405.
22 L. Isa, F. Lucas, R. Wepf and E. Reimhult, *Nat. Commun.*, 2011, **2**, 1–9.
23 A. Stocco, G. Su, M. Nobili, M. In and D. Y. Wang, *Soft Matter*, 2014, **10**, 6999–7007.
24 K. Larson-Smith, A. Jackson and D. C. Pozzo, *Langmuir*, 2012, **28**, 2493–2501.
25 H. D. Jia, I. Grillo and S. Titmuss, *Langmuir*, 2010, **26**, 7482–7488.
26 M. Moglianetti, Q. K. Ong, J. Reguera, K. Harkness, M. Mameli, A. Radulescu, J. Kohlbrecher, C. Jud, D. Svergun and F. Stellacci, *Chem. Sci.*, 2014, **5**, 1232–1240.
27 C. Stefaniu, M. Chanana, H. Ahrens, D. Y. Wang, G. Brezesinski and H. Mohwald, *Soft Matter*, 2011, **7**, 4267–4275.
28 D. C. E. Calzolari, D. Pontoni, M. Deutsch, H. Reichert and J. Daillant, *Soft Matter*, 2012, **8**, 11478–11483.
29 L. Isa, D. C. E. Calzolari, D. Pontoni, T. Gillich, A. Nelson, R. Zirbs, A. Sanchez-Ferrer, R. Mezzenga and E. Reimhult, *Soft Matter*, 2013, **9**, 3789–3797.
30 K. A. Tay and F. Bresme, *J. Am. Chem. Soc.*, 2006, **128**, 14166–14175.
31 F. Bresme and M. Oettel, *J. Phys.: Condens. Matter*, 2007, **19**, 413101.
32 R. K. Thomas and J. Penfold, *Curr. Opin. Colloid Interface Sci.*, 1996, **1**, 23–33.
33 J. Penfold and R. K. Thomas, *J. Phys.: Condens. Matter*, 1990, **2**, 1369–1412.
34 C. A. Rezende, J. Shan, L. T. Lee, G. Zalczer and H. Tenhu, *J. Phys. Chem. B*, 2009, **113**, 9786–9794.
35 M. Ujihara, K. Mitamura, N. Torikai and T. Imae, *Langmuir*, 2006, **22**, 3656–3661.

36 A. M. Jackson, J. W. Myerson and F. Stellacci, *Nat. Mater.*, 2004, **3**, 330–336.
37 A. Verma, O. Uzun, Y. H. Hu, Y. Hu, H. S. Han, N. Watson, S. L. Chen, D. J. Irvine and F. Stellacci, *Nat. Mater.*, 2008, **7**, 588–595.
38 A. Centrone, E. Penzo, M. Sharma, J. W. Myerson, A. M. Jackson, N. Marzari and F. Stellacci, *Proc. Natl. Acad. Sci. U. S. A.*, 2008, **105**, 9886–9891.
39 C. Singh, P. K. Ghorai, M. A. Horsch, A. M. Jackson, R. G. Larson, F. Stellacci and S. C. Glotzer, *Phys. Rev. Lett.*, 2007, **99**, 226106.
40 H. Kim, R. P. Carney, J. Reguera, Q. K. Ong, X. Liu and F. Stellacci, *Adv. Mater.*, 2012, **24**, 3857–3863.
41 Q. K. Ong, J. Reguera, P. J. Silva, M. Moglianetti, K. Harkness, M. Longobardi, K. S. Mali, C. Renner, S. De Feyter and F. Stellacci, *ACS Nano*, 2013, **7**, 8529–8539.
42 A. Nelson, *J. Appl. Crystallogr.*, 2006, **39**, 273–276.
43 P. Pieranski, *Phys. Rev. Lett.*, 1980, **45**, 569–572.
44 B. P. Binks, *Curr. Opin. Colloid Interface Sci.*, 2002, **7**, 21–41.
45 D. M. Andala, S. H. R. Shin, H. Y. Lee and K. J. M. Bishop, *ACS Nano*, 2012, **6**, 1044–1050.
46 P. Ionita, A. Volkov, G. Jeschke and V. Chechik, *Anal. Chem.*, 2008, **80**, 95–106.
47 P. E. Laibinis and G. M. Whitesides, *J. Am. Chem. Soc.*, 1992, **114**, 1990–1995.
48 W. D. Luedtke and U. Landman, *J. Phys. Chem. B*, 1998, **102**, 6566–6572.
49 T. Pradeep and N. Sandhyarani, *Pure Appl. Chem.*, 2002, **74**, 1593–1607.
50 N. Zheng, J. Fan and G. D. Stucky, *J. Am. Chem. Soc.*, 2006, **128**, 6550–6551.